Chapter 9
Optical Coherence Tomography

Paolo Frezzotti

Optical coherence tomography (OCT) is the most sensitive and promising diagnostic technique for detecting damage to optic nerve fibres. OCT is a modern imaging technique based on analysis of semicoherent radiation reflected by the structure of the tissue analysed. The high resolution possible with OCT (about 2 μm versus 150 μm with ultrasonometry) enables noninvasive imaging of the anterior chamber, retinal layers, choriocapillaris, retinal pigmented epithelium (RPE) and optic nerve/lamina cribrosa. The method is based on light, which unlike sound waves used in B-mode ultrasonography does not require contact with the tissue to be examined. It measures the delay in the echo and the intensity of diffused light, that is, the light reflected by tissue microstructure, using a wavelength of about 820 nm. This low coherence, near-infrared beam is projected by a superluminescent diode. The echo propagation times of the light reflected by the tissue are compared with those of the same beam reflected from a reference mirror at a known distance. The OCT system combines the pulses of light reflected by the eye (e.g. the retina) and the mirror, creating interference that is measured with a photodetector. Although the light reflected by the tissue is composed of multiple echoes, the distance travelled is determined by changes in mirror distance. The lag time of the reference light is used to deduce the thickness of the structures through which the light passed. Time-domain OCT is a technique by which movement of the mirror enables repeated scans at different depths (a single coherence measurement on a single structure at a given depth is called an A-scan). Maximum scan rate can be 17,000 A-scans/s, providing a one-dimensional measurement, which is then processed in two dimensions (B-scan) giving an image of the different tissue layers at the point analysed. The resulting section is called a "tomogram" (Fig. 9.1), visualised in real time using a scale of false colours representing the degree of backscattering of the light by the tissues at different depths.

P. Frezzotti
Ophthalmology Unit, University of Siena, Siena, Italy
e-mail: paolofrezzotti@paolofrezzotti.it

A. Ferreras (ed.), *Glaucoma Imaging*, DOI 10.1007/978-3-319-18959-8_9

The image is captured in a few seconds and requires steady fixation by the patient. A major advance consisted in analysing (by Fourier transform) the interference spectrum of the two reflected broad-spectrum beams, instead of measuring beam coherence. This Fourier spectral domain technique is much faster (simultaneous analysis at different depths), more accurate (2 μm) and therefore greatly reduces imaging times. Its main disadvantages are that the light cannot reach the retina if there are lens opacities and fixation must be extremely steady. However, it is worth bearing in mind that OCT images are not images of structure but a mathematical reconstruction built on a photograph of the fundus. The structures visualised are the result of selective absorption and selective reflection by the structure or the interface illuminated by the laser. This can depend on the type of structures (the most reflective are the retinal nerve fibre layer (RNFL), retinal pigmented epithelium and interplexiform cells) and on the direction of the incident ray (when structures are perpendicular to the ray, reflectivity is greater, indicated in red in OCT images).

Since 2001, analysis of the anterior segment using a wavelength of 1310 nm has been combined with analysis of eye fundus structures. This wavelength makes it possible also to examine the iris-corneal angle. The OCT-Visante® instrument we used for this chapter performs 2048 scans/s with axial and transverse optical resolution of 18 and 60 μm, respectively, and an imaging time of 0.125 s. In any case, OCT enables qualitative, morphological (anterior chamber, retina and optic nerve head) and quantitative analysis providing thickness mapping in various sectors. It is reliable, easy to perform, contact-free, pain-free and has a short learning curve. The images can be analysed, quantified, compared with later images or with other images obtained, for example, by fluoroangiography or ICG. In this chapter, we consider the information that OCT offers for studying, classifying and monitoring glaucoma patients through:

1. Anterior pole evaluation
2. Retinal nerve fibre layer and optic nerve head analysis
3. Ganglion cell analysis
4. Lamina cribrosa assessment

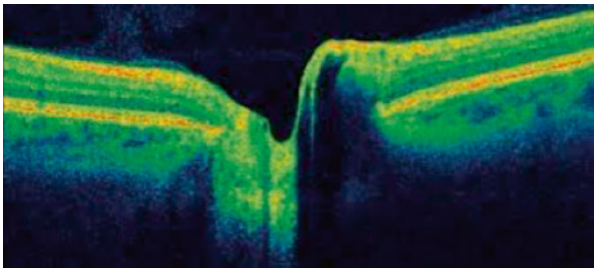

Fig. 9.1 Tomogram based on scale of false colours

9.1 Anterior Pole Evaluation

The Visante OCT instrument enables visualisation of the form, site and position of anterior chamber components and defines and measures the distances between them. The software automatically eliminates distortion induced by optical transmission factors. Various measurements can be obtained from the images: CA depth, angle to angle, chamber angle amplitude, pupil diameter and lens curvature.

In glaucoma, OCT of the anterior chamber is of special interest for assessing the amplitude and conformation of the angle, complementing gonioscopic evaluation. The anterior chamber angle is the junction between the iris root and the cornea. An important anatomical landmark for evaluating the angle is the scleral spur, which is the connecting point between the posterior curvature of the cornea and the curvature of the sclera. The trabecular meshwork and Schwalbe's line are located anterior to the scleral spur, whereas the iris root and the ciliary body are located posterior to it. Once the scleral spur is identified, the position of the iris relative to the scleral spur is checked. If the iris is posterior to the scleral spur, the angle is open, whereas if the iris is anterior to the spur, the angle is either narrow or closed.

The following figures show different clinical conditions detected by Visante OCT:

OCT is a useful tool for evaluating filtering blebs or glaucoma drainage devices in the postoperative period. Clinically, blebs can be described as diffuse, cystic, encapsulated or flat. However, these descriptions are subjective and there may be cases in which clinical appearance does not correlate with bleb function. Visualising intrableb morphology with anterior segment imaging may therefore enhance our understanding of different surgical outcomes and wound healing. The following figures show certain aspects of conjunctival blebs after trabeculectomy.

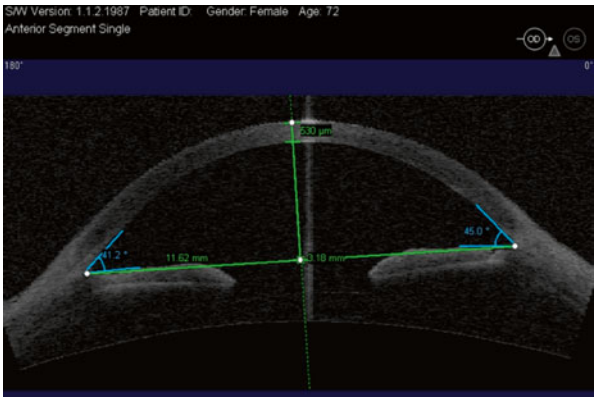

Fig. 9.2 Measurement of horizontal and vertical anterior chamber diameters, angle amplitude and corneal thickness

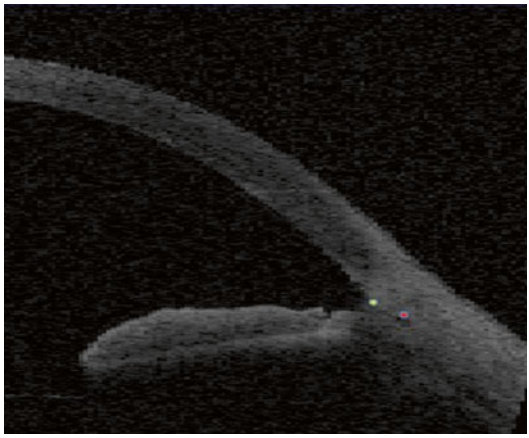

Fig. 9.3 Anatomical aspects of the anterior chamber angle. *Red dot*: scleral spur connecting point between the posterior curvature of the cornea and the curvature of the sclera. *Yellow dot*: linear distance of 500 μm anterior to the scleral spur marking the site of the trabecular meshwork

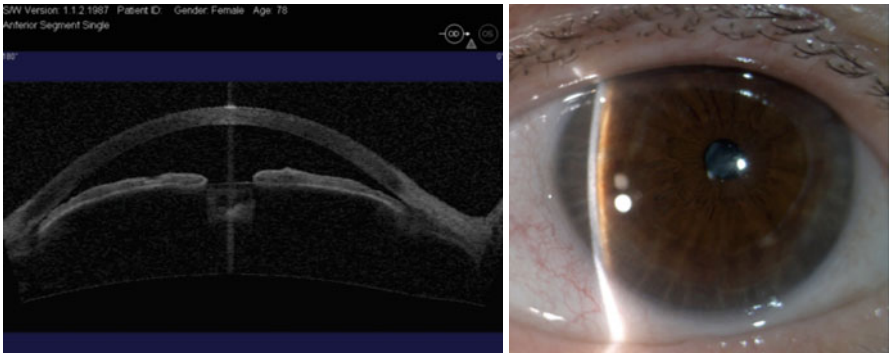

Fig. 9.4 Narrow angle. Clinical feature with Van Herick sign. OCT image shows temporal and nasal closure of the angle

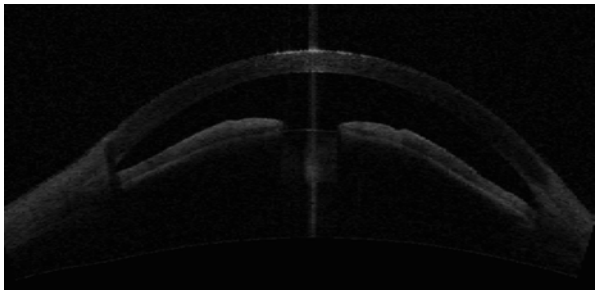

Fig. 9.5 Narrow angle. The chamber angle is closed. Note synechia at the base of the angle caused by inflammation arising during closure crises

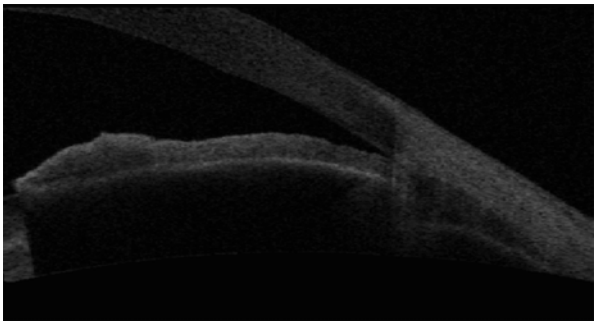

Fig. 9.6 Narrow angle. The angular recess is present. The situation worsens during midriasis and progressive apposition will lead to chronic closure (Mapstone's hypothesis of two-stage closure of the angle)

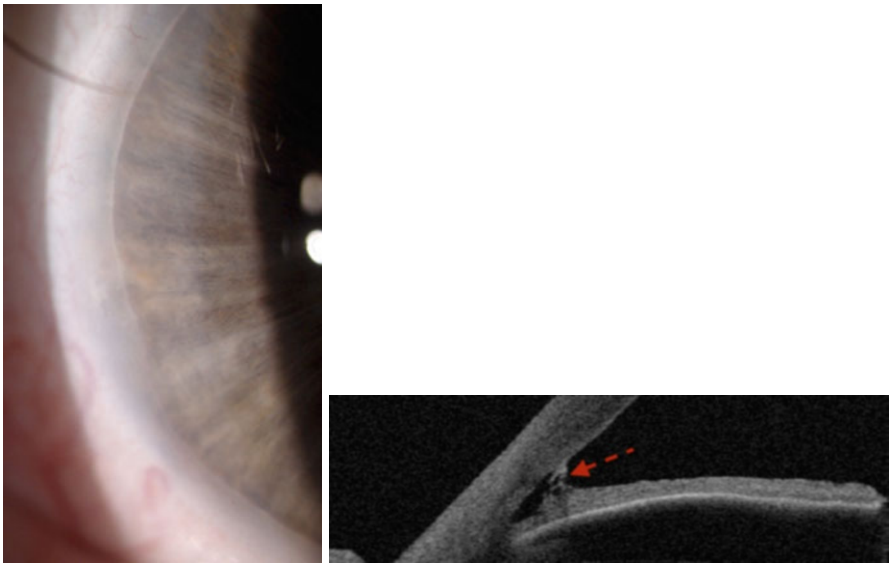

Fig. 9.7 Anxenfeld's anomaly. Anterior segment photo and OCT image showing posterior embryotoxon with iris processes that extend to Schawalbe's line (*red dotted arrow*). The changes to the angle affect the entire angle and the iris usually inserts anteriorly and obscures the scleral spur

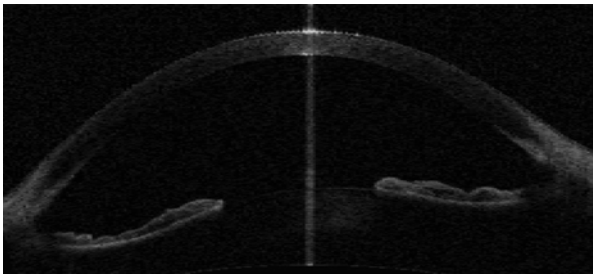

Fig. 9.8 Pigment dispersion glaucoma. OCT image showing concave iris with underlying iris-zonula contact that during miosis-midriasis causes degranulation and dispersion of pigment. Indeed, the pathogenetic event of this syndrome has extensive close contact between iris and lens that by causing contact at the pupil leads to accumulation of aqueous humour in the anterior chamber, pressure imbalance and iris concavity (inverse pupillary block)

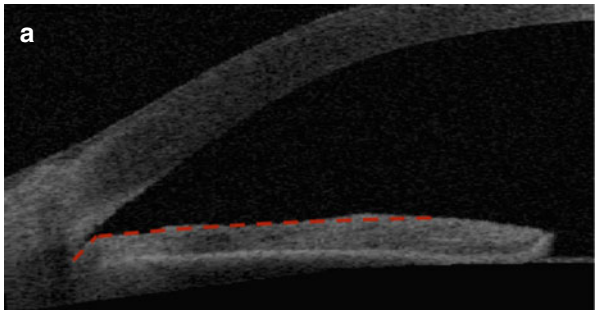

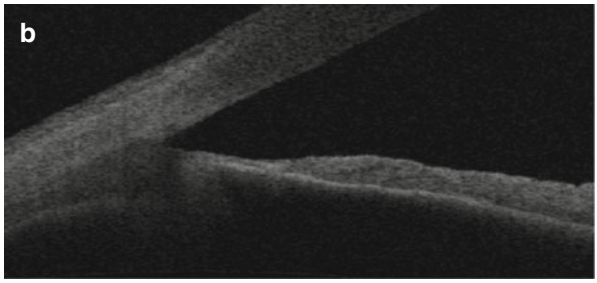

Fig. 9.9 (**a**) Plateau iris. OCT image showing a flat iris profile with anterior insertion (*red dotted line*) and anterior rotation of the ciliary bodies which raise and push the iris root towards the angle. (**b**) Plateau iris. OCT image showing the angle of (**a**) after Argon laser iridoplasty treatment. The angle appear open now

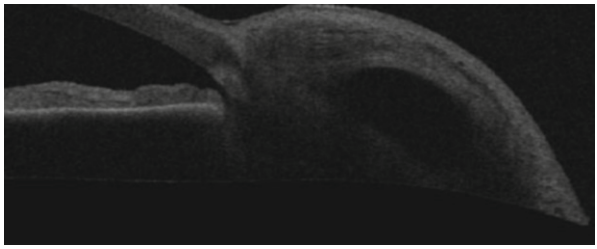

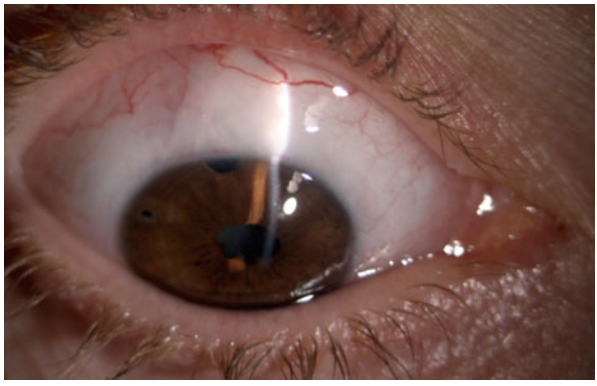

Fig. 9.10 Type L bleb (low reflectivity). OCT image showing surgical path from anterior chamber to the evident bleb. The low reflectivity of the conjunctiva indicates imbibition of aqueous humour by the bleb and success of the operation. The biomicroscope image shows a wide raised bleb

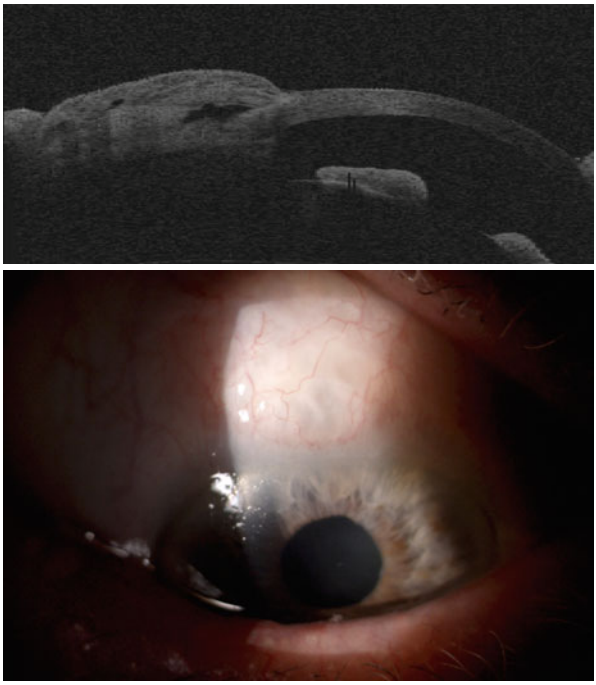

Fig. 9.11 Type H bleb (high reflectivity). OCT image showing that the bleb is functioning. The scleral surgical path is evident. The high reflectivity of the conjunctiva over the bleb indicates reduced imbibition. The biomicroscope image shows a wide functioning bleb

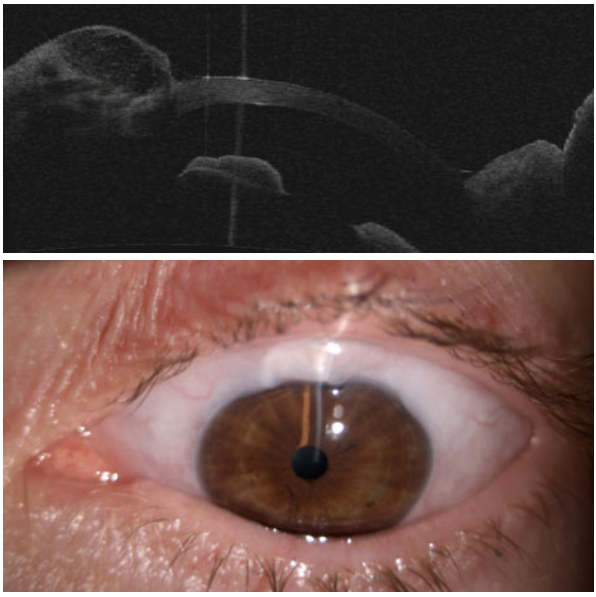

Fig. 9.12 Type E bleb (encapsulated or cystic). OCT image showing thin conjunctiva and iridectomy. Function may be relative and variable. The biomicroscope image shows a thin raised bleb with a cystic appearance; it maintains relative function in the nasal sector

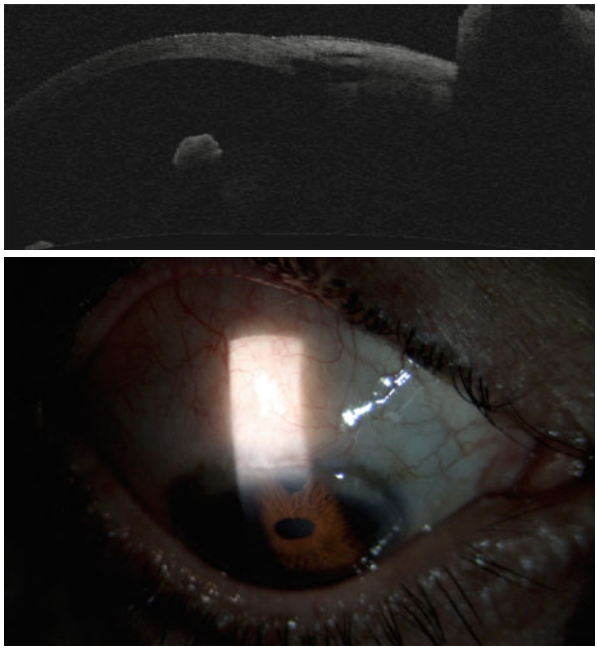

Fig. 9.13 Type F bleb (flat). OCT image showing opening of the anterior chamber but the surgical path is not visible. The bleb is absent and not functioning. The biomicroscope image shows a flat bleb with absence of filtration

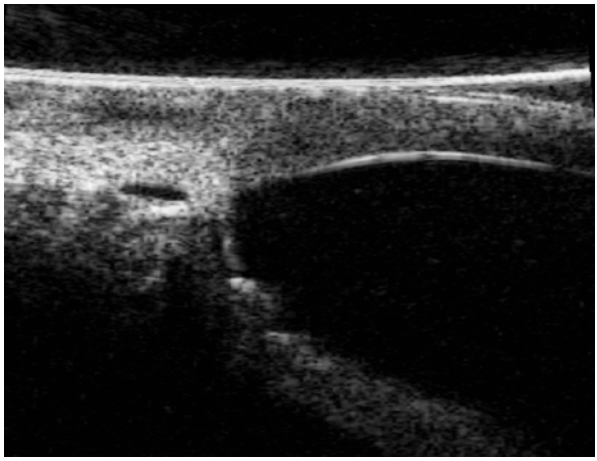

Fig. 9.14 Canaloplasty: detail of the Schlemm canal stretched by a prolene suture, which when correctly tensioned, improves its drainage capacity

9.2 Retinal Nerve Fibre Layer and Optic Nerve Head Analysis

The new generations of spectral-domain OCT have improved sensitivity in detecting structural changes in retinal nerve fibres and optic nerve head (ONH) morphology, achieving a resolution of 2 μm. The OCT software package includes 19 scan and 18 analysis protocols. Together they make it possible to analyse the optic disc, the nerve fibre layer and the macula with the same instrument. The video camera enables fundus examination in action and simultaneous saving of video images and scans. OCT of the optic nerve enables detection of retinal nerve fibre damage and changes in time by statistical comparison of different OCT images from the same patient.

OCT examination print-out consists of various parts (Fig. 9.15):

1. Table of parameters compared with a normative database
2. Topographic map of retinal nerve fibre layer (RNFL) thickness
3. Map of RNFL deviation from normal values
4. Neuroretinal rim thickness
5. RNFL TSINIT graph of measurements in the area analysed
6. Mean RNFL thickness in each quadrant
7. Horizontal and vertical B-scans
8. Calculation of RNFL thickness in the circle of interest

In the protocol, mean RNFL thickness is visualised using a white-green-yellow-red colour code. Colour coding indicates the particular position of the A-scan in the graph, the quadrant mean values and the clock-position in the circular graphs, and right and left eye columns of the table of data. In the age-matched normal population, the percentiles regard each specific measurement of RNFL thickness, in the following way:

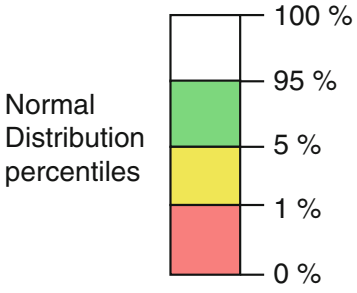

- The thinnest 1 % of measurements fall in the red area. Measurements in red are considered outside normal limits (red <1 %, outside normal limits).
- The thinnest 5 % of measurements fall in or below the yellow area (1 % < yellow < 5 %, suspect).

- 90 % of measurements fall in the green area (5 % < green < 95 %).
- The thickest 5 % of measurements fall in the white area (white > 95 %).

Of the ONH parameters examined, those that revealed progressive changes in the manifestations of glaucoma were vertical thickness of the neuroretinal rim, overall area of the rim and vertical C/D ratio. However, these parameters do not help distinguish initial from advanced glaucoma. For this purpose, OCT measurements of RNFL parameters, especially average RNFL thickness, RNFL thickness in the lower temporal zone and RNFL in the lower quadrant (Fig. 9.16) were more useful.

Although diagnosis and follow-up assessments of glaucoma are based on anatomical and functional damage, the relationship between the two has not yet been clearly defined. Studies seeking a connection between visual field and anatomical damage have begun to link this data. An understanding of the relation between structure and function in glaucoma could facilitate efficacy evaluation of structural and functional tests for early diagnosis of glaucoma damage and for accurate staging. As damage progresses, there is a correlation between worsening of both the optic disc and the disease; structural changes seem to be detectable before functional ones. Rao et al. (2011) compared treated and untreated patients with POAG, finding that in the course of the disease most patients (>50 %) deteriorated prevalently from a structural point of view, about 30 % deteriorated only functionally and about 10 % deteriorated structurally and functionally. More recent studies showed that when applied to slight-moderate glaucoma, spectral-domain OCT ensures a better correlation between structure and function than time-domain OCT. However, one parameter explains only 30 % of the trend of the other. Thus it is possible to be faced with different clinical situations, as illustrated in the following examples.

Anatomical variations in the optic nerve are so numerous that they cannot all be included in the database used by OCT software. This may lead to classification of abnormal ONH parameters for absolutely normal RNF and white-on-white perimetry parameters. In such situations, the RNFL classification must be preferred, monitoring any changes through careful follow-up (Fig. 9.17).

When faced with altered anatomical ONH and RNFL parameters and high intraocular pressure without visual field damage according to conventional white-on-white perimetry, we have preperimetric glaucoma. Besides monitoring the patient we can consider beginning therapy, especially when anatomical damage is substantial (Figs. 9.18 and 9.19).

When structural damage is associated with functional visual field damage, we have initial glaucoma. In this stage, ONH and RNFL damage is greater than visual field damage, especially in young patients.

There are cases in which alteration of ONH parameters and visual field is associated with normal RNFL thickness. Indeed, one may encounter patients with OCT evidence of damage as well as visual field damage in one eye, but only visual field damage in the other eye. This is sufficient for a diagnosis of glaucoma in both eyes (Fig. 9.21).

When the severity of glaucoma increases to the stage of moderate, it can present with greater OCT evidence of structural damage than functional visual field damage. In this case, anatomical damage can provide important indications of how functional damage could evolve (Fig. 9.22). Another possible presentation shows greater concordance of structural ONH damage and RNFL thickness with visual field damage (Fig. 9.23).

Imaging of structural damage is also important in advanced forms of glaucoma, although assessment of clinical condition and progression are essentially based on functional visual field data. Structural damage to RNFL thickness does not go below 50 μm, which corresponds to visual field areas of absolute scotoma. In these forms of glaucoma, the concordance between anatomical and functional damage may vary, but unlike in the above situations, the visual field usually shows greater evidence of damage. Examples follow (Figs. 9.24 and 9.25).

Another major use of OCT in assessing progression of glaucoma is that proposed by guided progression analysis (GPA), a programme of analysis of progression based on data obtained from OCT images (Fig. 9.26). As shown in the figure, the upper part of the OCT print-out shows images of ONH fibre thickness, and below it images showing changes in fibre thickness between OCT examinations. When a first reduction (possible change) is detected, it is highlighted in yellow (Fig. 9.27); if it is confirmed in the next OCT (probable change) it is highlighted in red; if an increase is detected, it is highlighted in violet (Fig. 9.27). Further down we find graphs representing longitudinal changes in RNFL thickness and in the overall mean value for the upper and lower sectors; changes in mean cup/disc ratio during follow-up are represented in the same way. In the lower part of the print-out on the left, we have a graph with RNFL thickness profile with the same colour coding for changes over time; on the right we have a window in which progression probability is indicated in an immediate and readily understood manner by summary boxes containing parameters that may vary significantly. It is important to bear in mind that like other types of morphological analysis of fibres, OCT, too, is subject to certain artefacts: strong interference at the vitreous-retinal interface and intraretinal oedema can deceive the automatic segmentation algorithm, creating false measures and increasing test-retest variability.

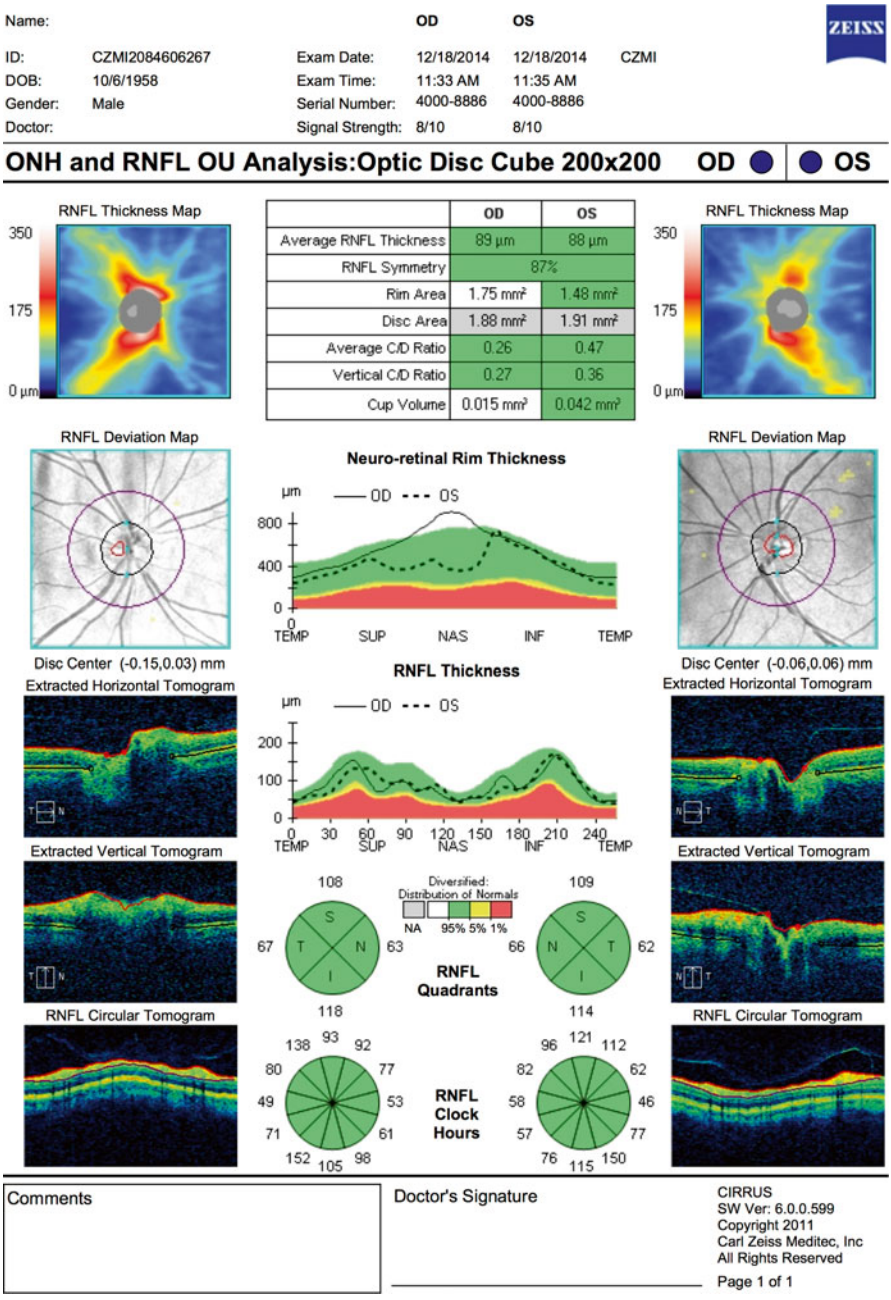

Fig. 9.15 Print-out of OCT examination of the optic nerve head and RNFL

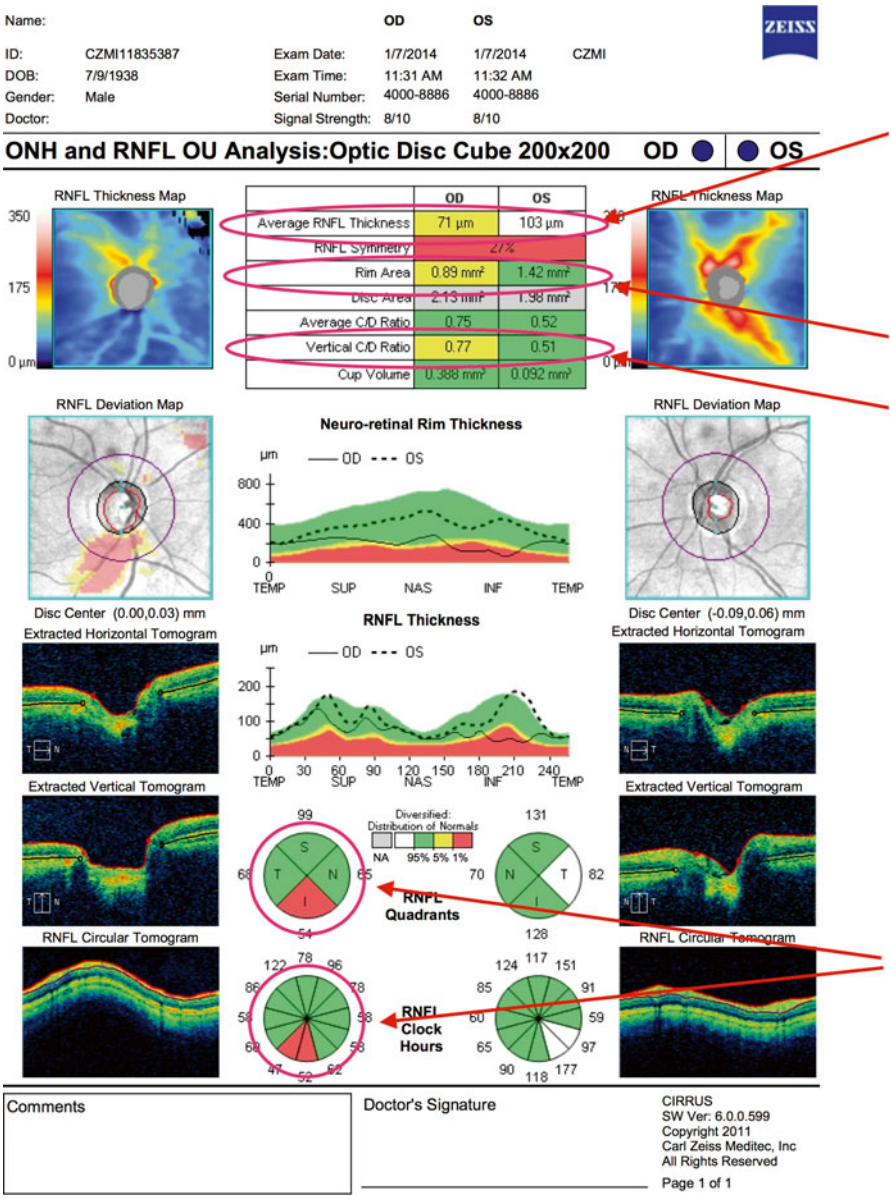

Fig. 9.16 OCT print-out – the most useful parameters (*circled*) for differentiating normal and glaucomatous patients are: vertical thickness of neuroretinal rim, overall area of rim, vertical C/D ratio, average RNFL thickness, RNFL thickness in lower temporal zone and in the lower quadrant

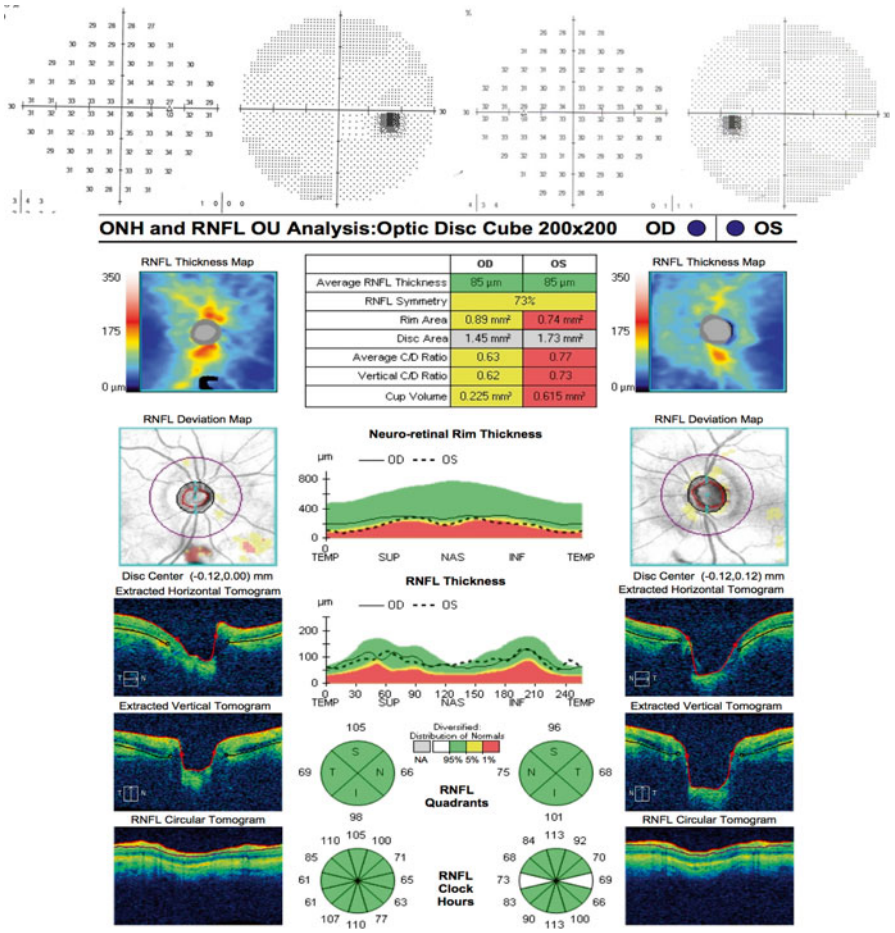

Fig. 9.17 RNFL parameters are normal, whereas ONH parameters (rim area, vertical and average C/D ratio, cup volume) are abnormal. In this case, it is sufficient to monitor the patient

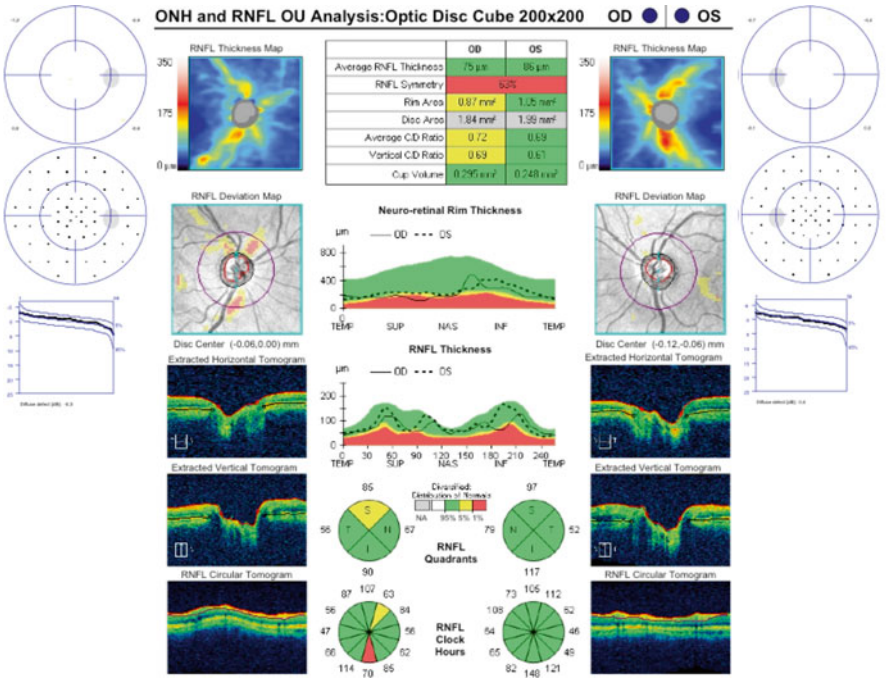

Fig. 9.18 ONH and RNFL parameters are slightly altered and Octopus perimetry seems normal. In deciding whether or not to begin therapy, it is also important to consider risk factors. The patient should be monitored

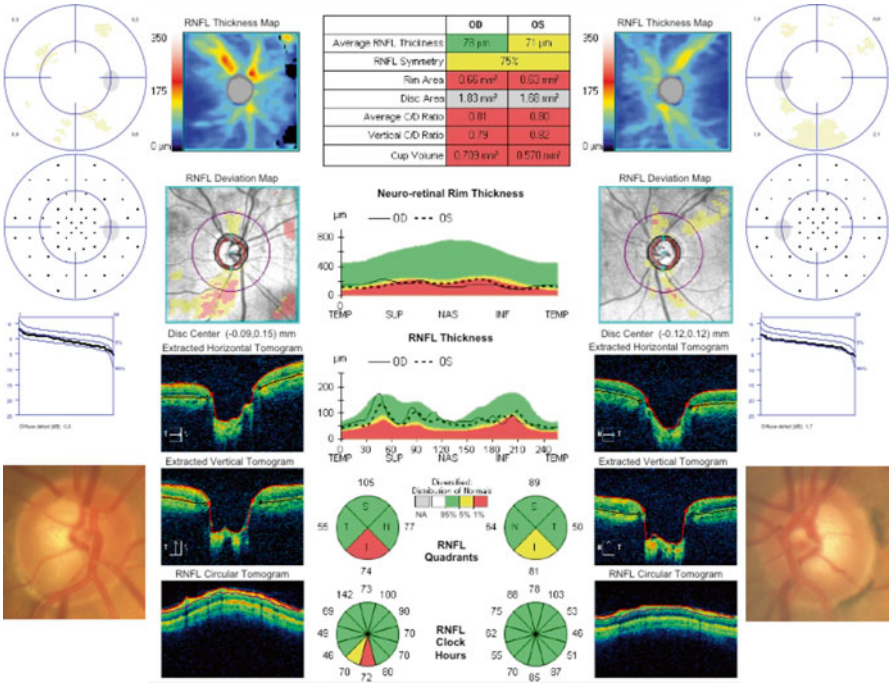

Fig. 9.19 ONH and RNFL parameters are altered in both eyes, especially in the right eye. Octopus perimetry is again normal. In this case with high intraocular pressure, we have preperimetric glaucoma and hypotonic therapy should be started

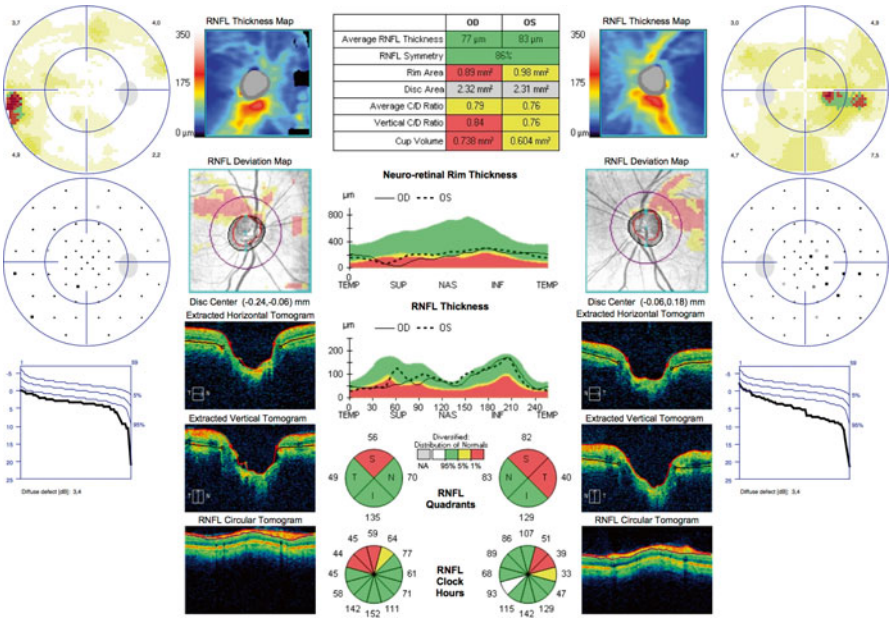

Fig. 9.20 ONH and RNFL parameters are altered in both eyes, especially in the left eye, and Octopus perimetry shows damage in both eyes. This case, in which there is good agreement between structural damage detected by OCT and perimetric damage, can be classified as initial glaucoma. In such patients, perfect concordance between the two is rare. Hypotonic therapy should be begun and the patient monitored periodically

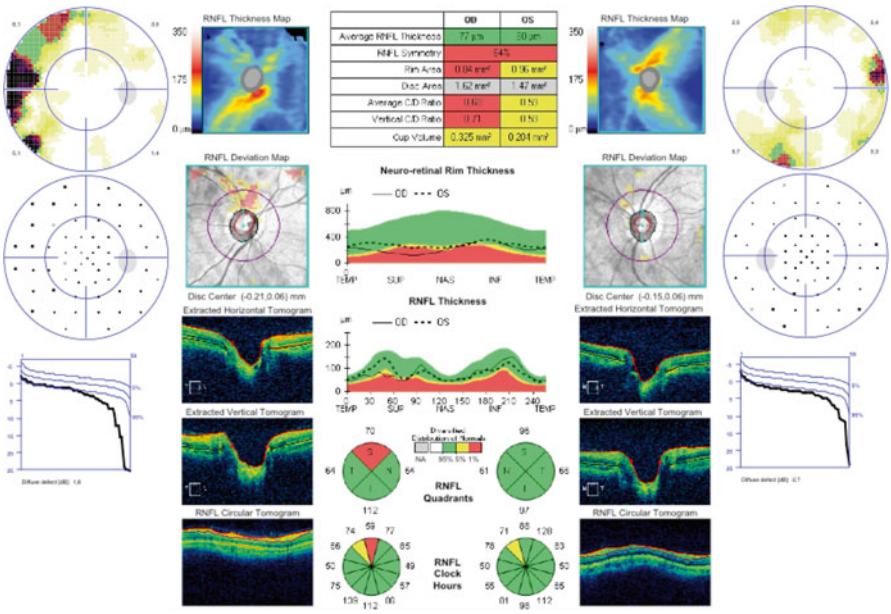

Fig. 9.21 ONH parameters are altered in both eyes, especially in the right eye, which also shows Octopus perimetry alterations. RNFL structural parameters detected by OCT are only altered in the right eye. In this case, we can also classify the left eye as glaucomatous due to perimetric damage, even in the absence of RNFL alterations

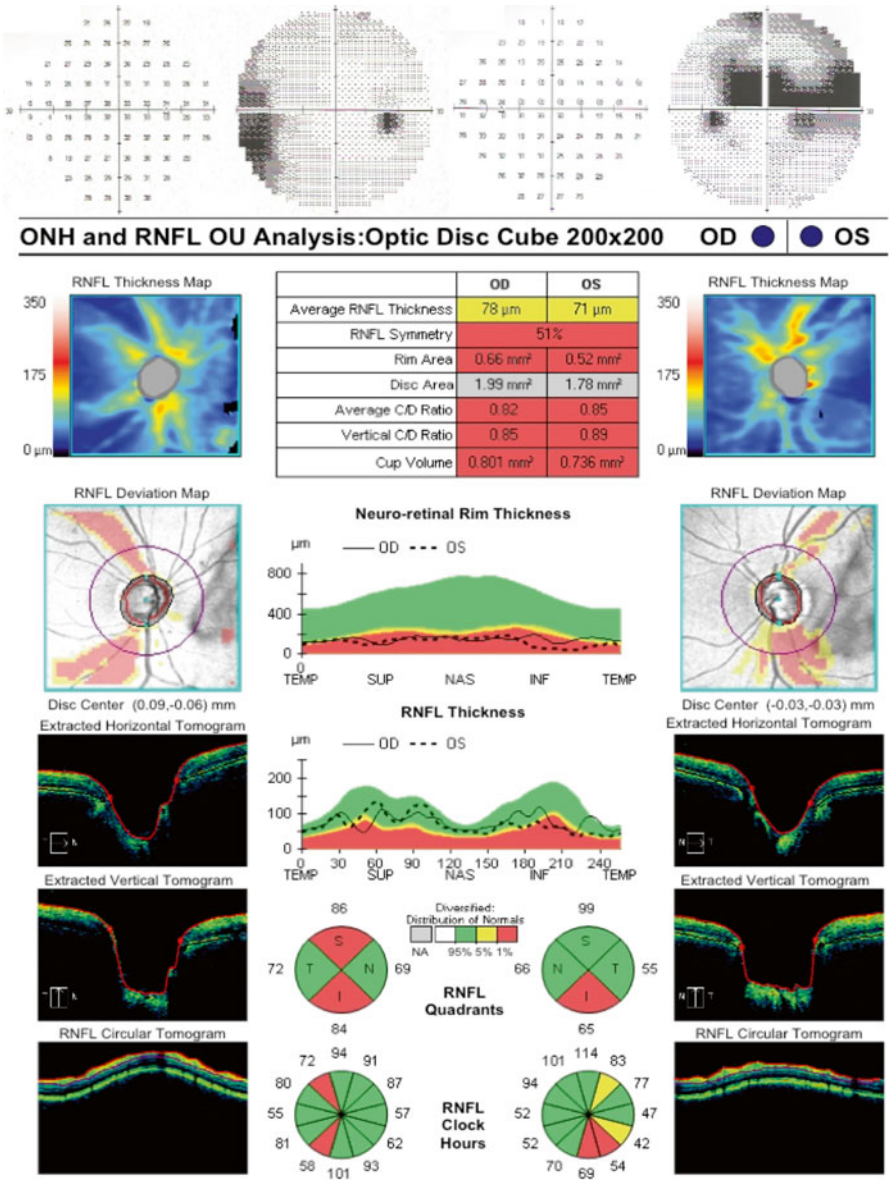

Fig. 9.22 ONH and RNFL parameters are altered in both eyes in more or less the same way. However, perimetry shows greater functional damage on the left. In such patients it is particularly useful to monitor regions that have structural damage but normal visual field

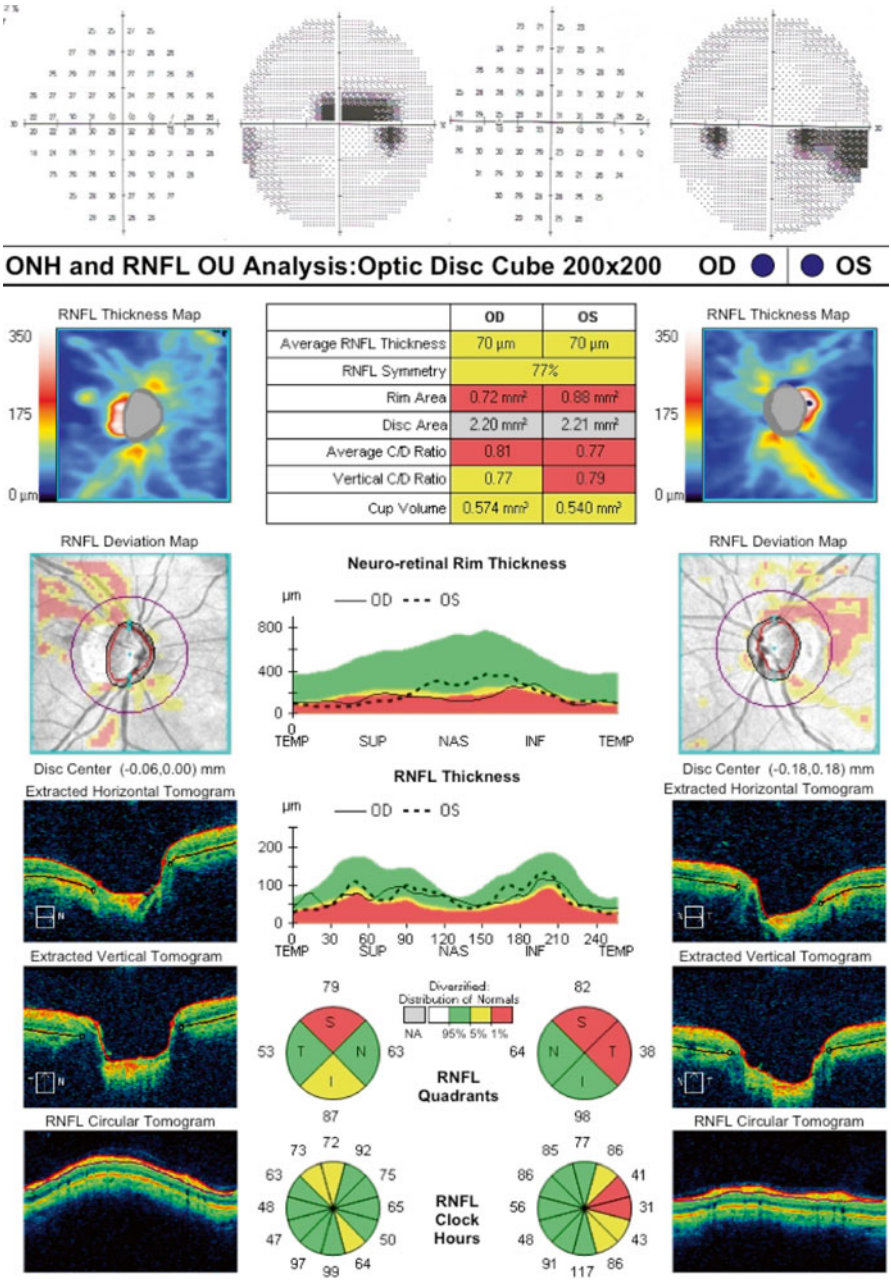

Fig. 9.23 ONH and RNFL parameters are altered in both eyes in more or less the same way. Perimetry confirms structural damage with good concordance. Progression of the disease should be carefully monitored by evaluating both anatomical and functional damage

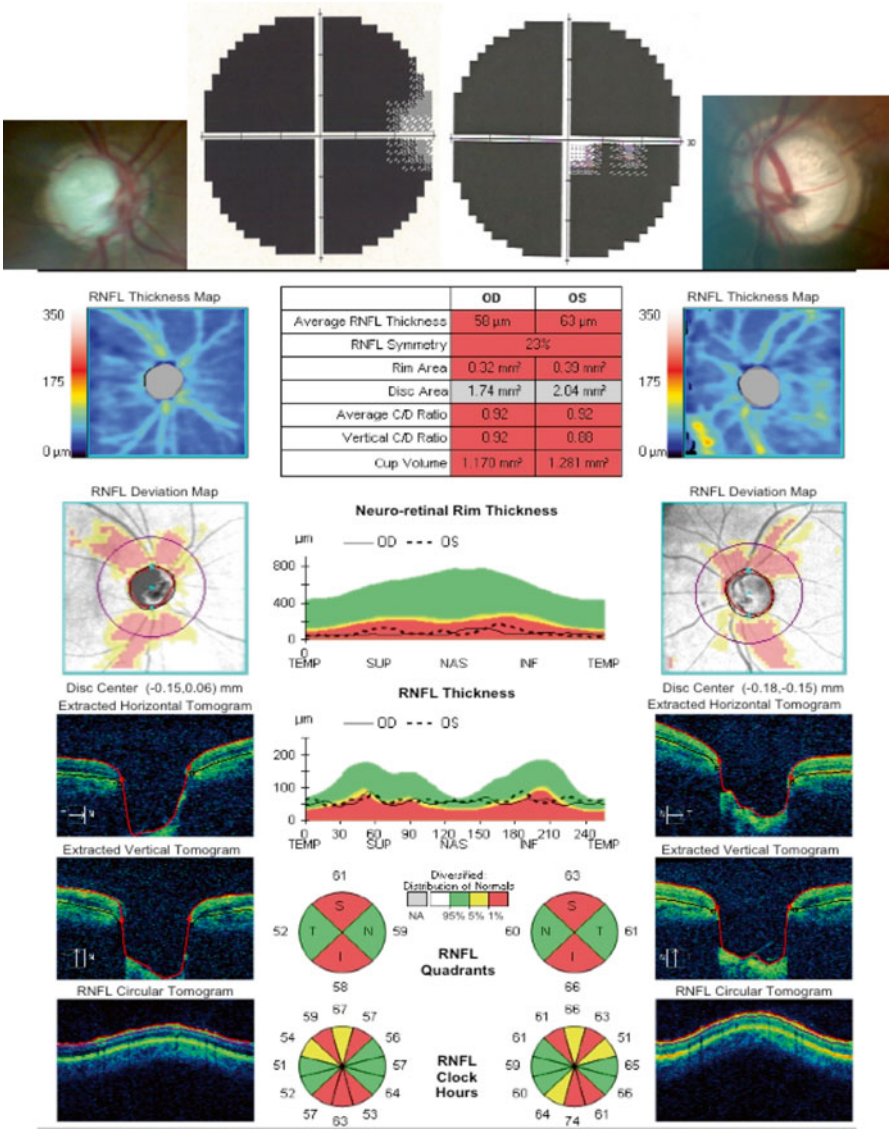

Fig. 9.24 Advanced glaucoma: ONH and RNFL parameters are severely altered in both eyes and more or less in the same manner. ONH morphological parameters are all pathological and average RNFL thickness of the right eye is 50 µm, although certain areas (nasal and temporal sectors) show RNFL thickness within normal limits. Perimetry amplifies the structural damage findings, showing visual field areas of the right and left eyes with VFIs of 1 % and 6 %, respectively. This is the terminal stage of the disease where functional damage outweighs OCT evidence of structural damage

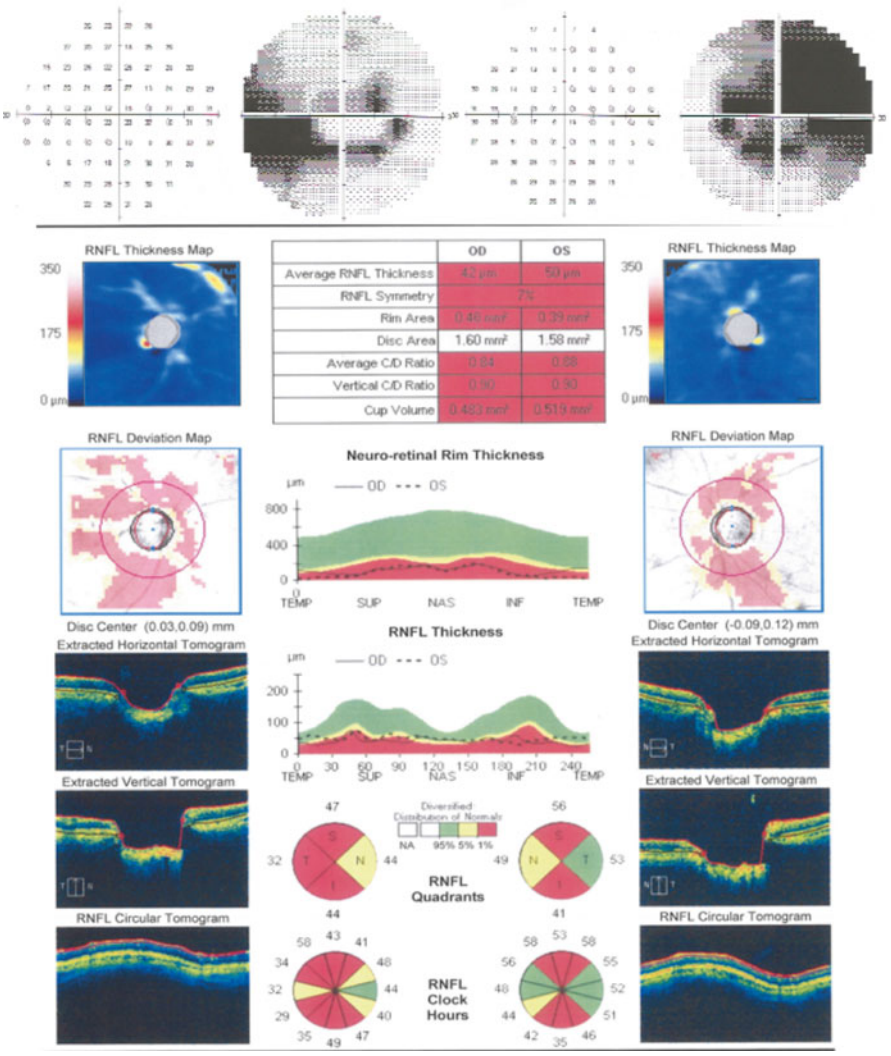

Fig. 9.25 Advanced glaucoma: ONH and RNFL parameters are severely altered in both eyes. ONH morphological parameters are all pathological and average RNFL thicknesses of the right and left eyes are 41 and 50 µm, respectively. Perimetry shows a good correlation with structural damage, revealing visual fields in line with clinical severity

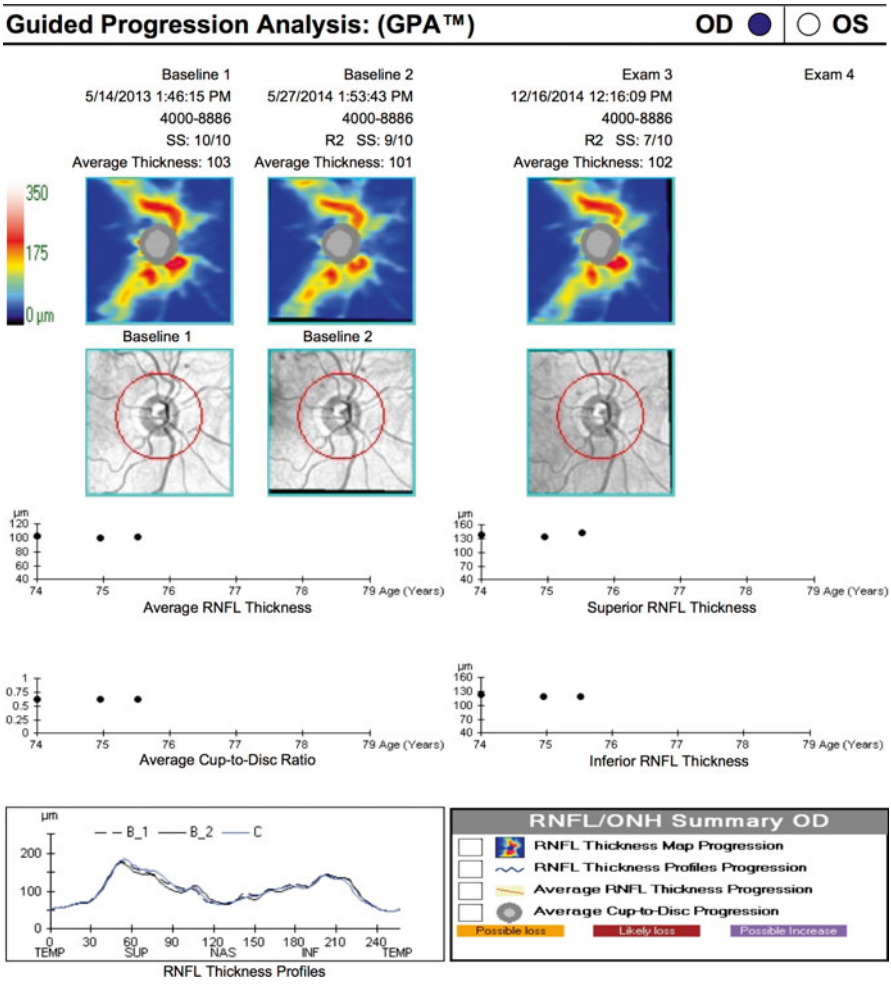

Fig. 9.26 Print-out of parameters used by GPA to monitor progression of glaucoma

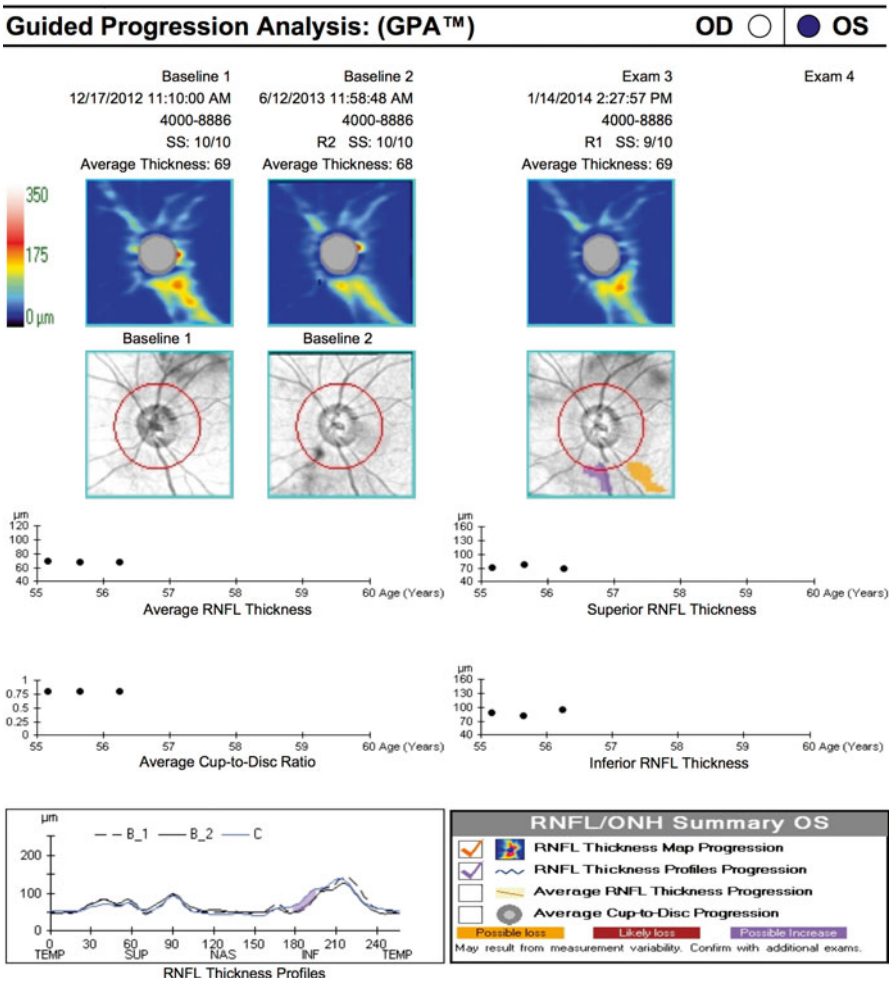

Fig. 9.27 Print-out of parameters used by GPA showing changes in fibre thickness during follow-up

9.3 Ganglion Cell Analysis

Spectral-domain OCT has proved useful for assessing glaucoma because it enables the ganglion cell complex (GCC) to be studied. The GCC consists of three layers (nerve fibre layer, ganglion cell layer and inner plexiform layer) containing axons, cell bodies and dendrites of ganglion cells, loss of which is typical of glaucoma optic neuropathy. Cross-sectional imaging of the macular area was performed using the Cirrus OCT macular cube (512×128). This acquisition protocol generates a cube through a 6 mm square grid of 128 B-scans, each consisting of 512 A-scans. A built-in GCC analysis algorithm detects and measures the thickness of the macular GCC in a 6×6×2 mm elliptical annulus centred on the fovea. The annulus has an inner vertical diameter of 1 mm, chosen to exclude parts of the fovea where the layers are very thin and difficult to detect accurately, and an outer vertical diameter of 4 mm, chosen to coincide with where the GCC again becomes thin and difficult to detect. The thickness values recorded are mean thickness, mean minimum thickness (thickness of the thinnest sector) and the topography of the macular region divided into six sectors: superior, inferior, superior and inferior temporal and superior and inferior nasal. Again, the data is first compared with a normative database in the form of maps, graphs and tables that use colours in the same manner as for the ONH protocol. GCC thicknesses in the normal range are represented by green backgrounds. The thinnest 5 and 1 % of measurements are represented by yellow and red backgrounds, respectively. The hypernormal (95th to 100th percentiles) pRNFL thicknesses are presented by a white colour (Fig. 9.28). Early glaucoma damage manifests with changes in the mean minimum thickness of the inferior temporal sector.

Continuous development and evolution of methods for measuring structure have helped researchers in their attempts to link structural evaluations with visual function. As already mentioned, many studies that examined the relation between structure and function in glaucoma have led to a simple linear (one-to-one) model linking structure (GCC thickness) and function (visual field sensitivity). However, other parameters such as wide anatomical variability, simultaneous presence of other local or systemic pathologies, or the entity of sight defects can influence structural measurements, such as RNFL and GCC thicknesses. We also have to consider that visual sensitivity expressed by the visual field reaches a plateau and does not increase indefinitely, even when GCC thickness is particularly large. Besides, a rapid decrease in visual sensitivity expressed by the visual field seems correlated with situations in which GCC thickness falls below a certain threshold. This indicates that nonlinear logistic analysis, as studied by many researchers, would be more appropriate for reliably linking this structural and functional data. Until this is achieved, I submit a series of conditions that can be useful in clinical practice.

When faced with high intraocular pressure and alterations in GCC anatomical parameters without conventional white-on-white perimetric evidence of visual field damage, we have preperimetric glaucoma. In such cases, besides monitoring the patient it is worth contemplating therapy, especially when anatomical damage is substantial (Fig. 9.29).

With progression of the disease, we have initial glaucoma when structural damage is associated with functional visual field damage. In this stage, one may be faced with situations in which GCC damage is congruous with functional damage as indicated by white-on-white perimetry (Fig. 9.30).

However, we are more likely to encounter cases in which ONH, RNFL and GCC damage is greater than visual field damage as detected by Humphrey perimetry (programme 30.2 and 10.2) or by Octopus perimetry (G1 and M), especially in young patients. Indeed, it is mainly in young patients that we find situations in which the difference between structure and function is much more accentuated. This is because young people have a high reserve of ganglion cells for the different areas of the visual field, so that structural damage may be greater than visual field damage (Fig. 9.31).

Also in more advanced forms of glaucoma, it is interesting to note that structural damage tends to be on average greater than perimetric damage. Patients with asymmetric damage, as shown in Figs. 9.32 and 9.33, are of special interest. Figure 9.30 showed a match between structure and function, both in the damaged and the undamaged (left) eye. In Fig. 9.31, structural and functional damages were congruous in both eyes. Indeed, MD was −17.6 dB and mean thickness 60 μm in the right eye, compared to −1.4 dB and 73 μm in the left eye.

In advanced forms of glaucoma, structural damage is also substantial, though assessment of clinical condition and progression are essentially based on functional visual field data. In fact it is often difficult to assess variations in structural damage when faced with major reductions in GCC thickness, as in the right eye shown below, in which structural damage is at a maximum and perfectly matches the functional damage detected by white-on-white Octopus perimetry. The major structural damage in the left eye provides an indication of the evolution of functional damage in time. In this example, we have extreme situations: MD −23.2 dB in the right eye coupled with a mean thickness of 44 μm, that is, correspondence of structural and functional damages, whereas MD 02.4 dB and 50 μm in the left eye show that structural damage is more evident than perimetric damage.

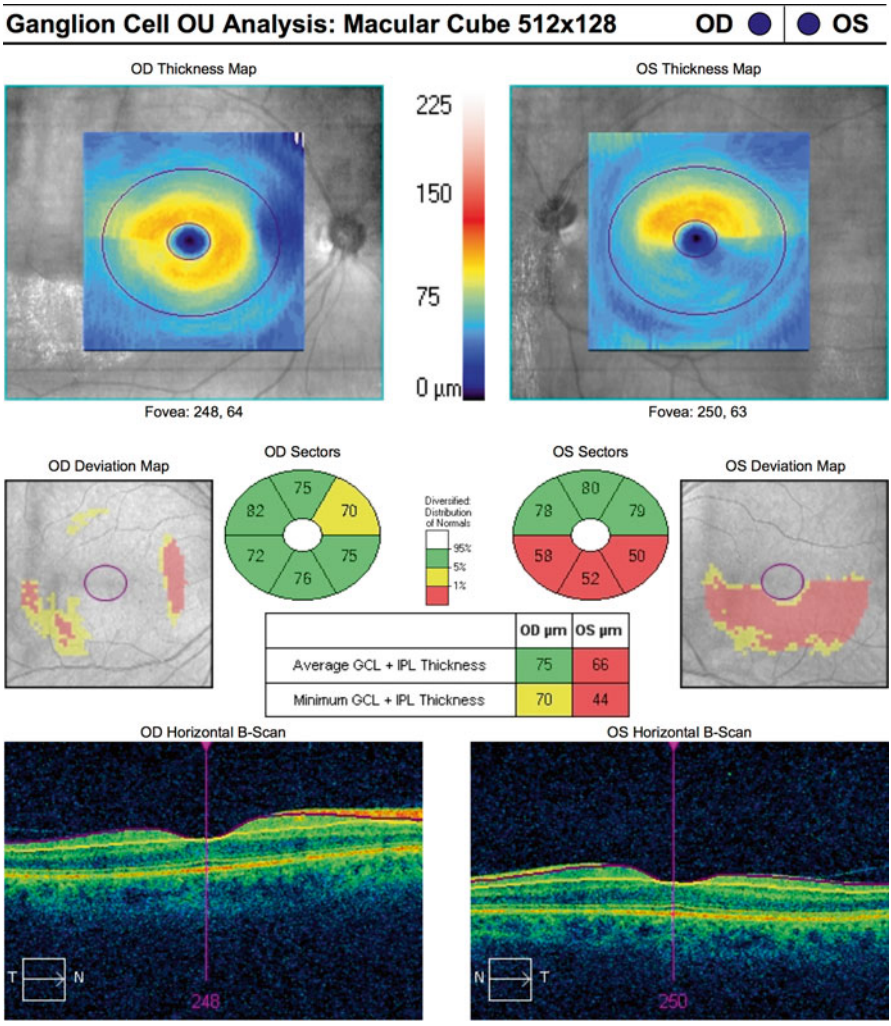

Fig. 9.28 Spectral-domain OCT analysis of retinal ganglion cells: thickness data is provided after comparison with a normative database in the form of maps, graphs and tables using colours in the same way as in the ONH protocol

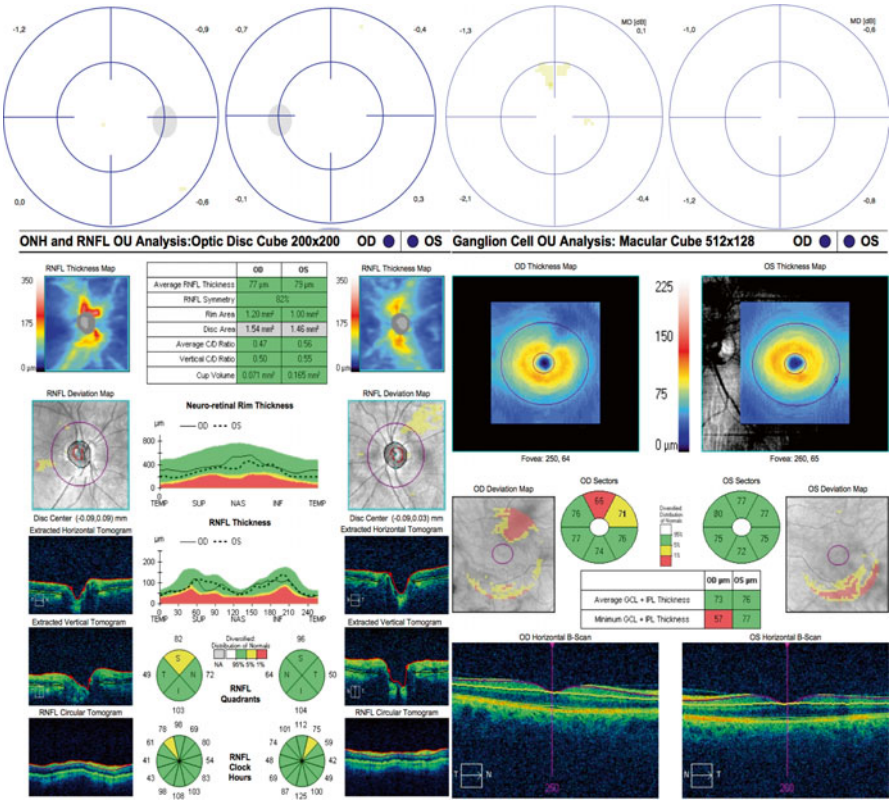

Fig. 9.29 GCC parameters are slightly altered and Octopus perimetry is normal. In this case, risk factors should also be considered when deciding whether to begin therapy. The patient should be monitored

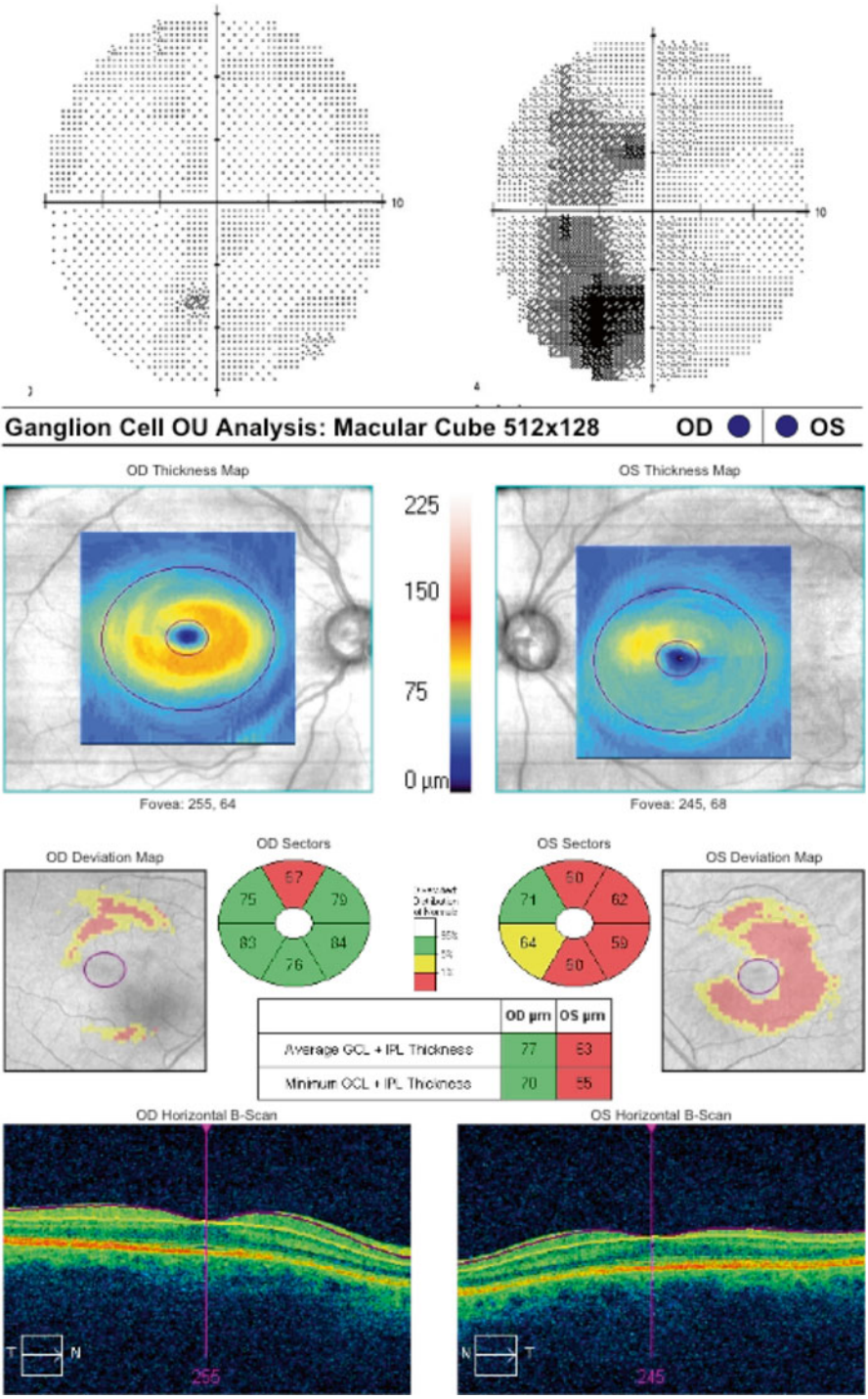

Fig. 9.30 GCC parameters are altered almost perfectly in line with severity and position indicated by Humphrey 10.2 perimetry. In these stages, structural damage can be detected earlier than functional damage

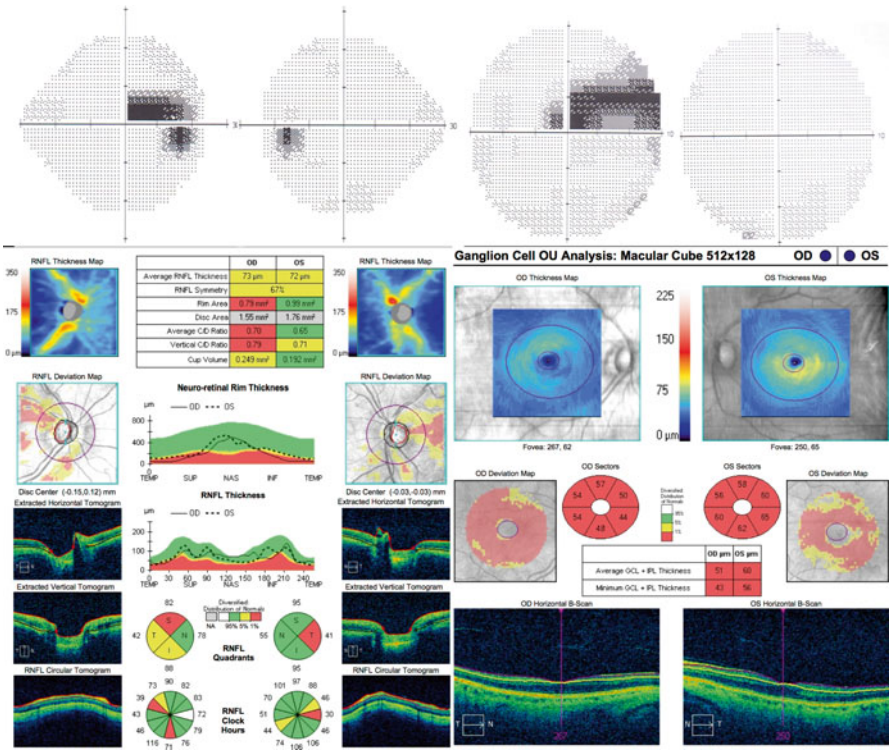

Fig. 9.31 ONH, RNFL and GCC parameters are altered more than those measured by Humphrey perimetry. Note that in the right eye there is structural and functional damage, though the former seems greater. In the left eye only structural damage is evident, and greatly precedes the appearance of functional damage as measured by Humphrey perimetry (24.2 and 10.2). In this case, it is important to begin therapy in both eyes, seeking an appropriate pressure target with patient risk factors in mind

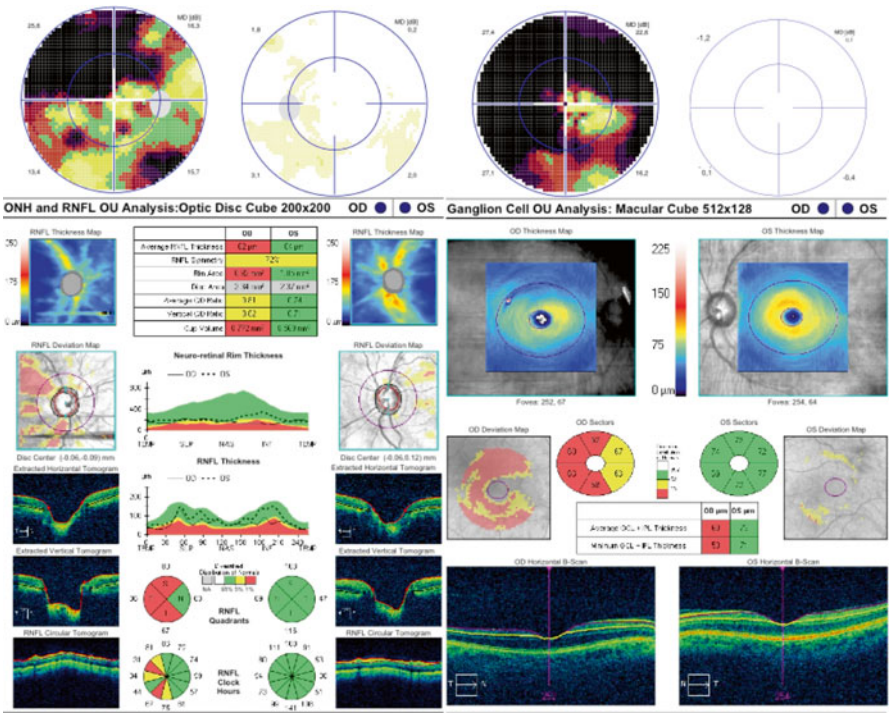

Fig. 9.32 Alterations in ONH, RNFL and GCC parameters matched functional damage as measured by Octopus perimetry. Note the interesting structural/functional congruence in both eyes

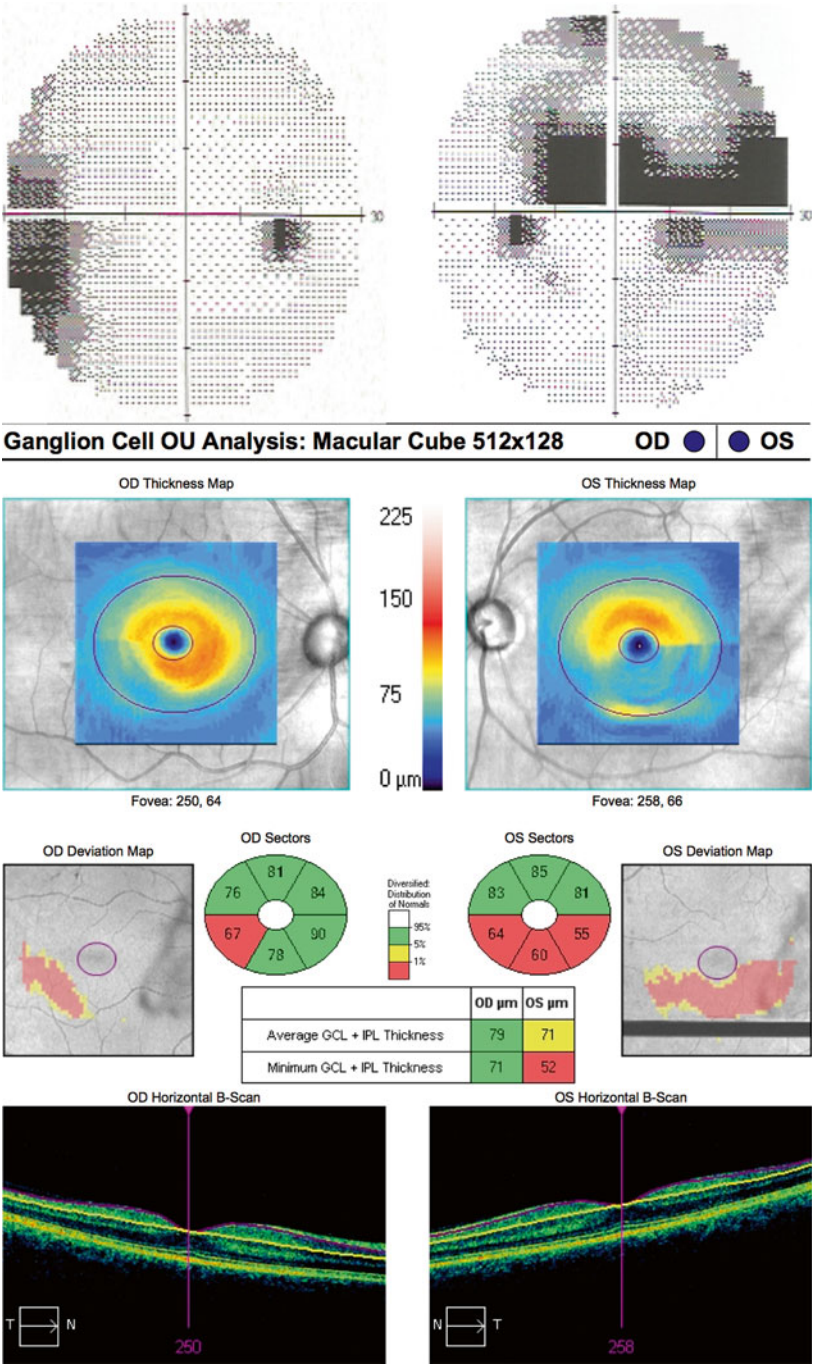

Fig. 9.33 GCC parameters are reduced and match evidence of functional damaged measured by Humphrey 30.2 perimetry in both eyes

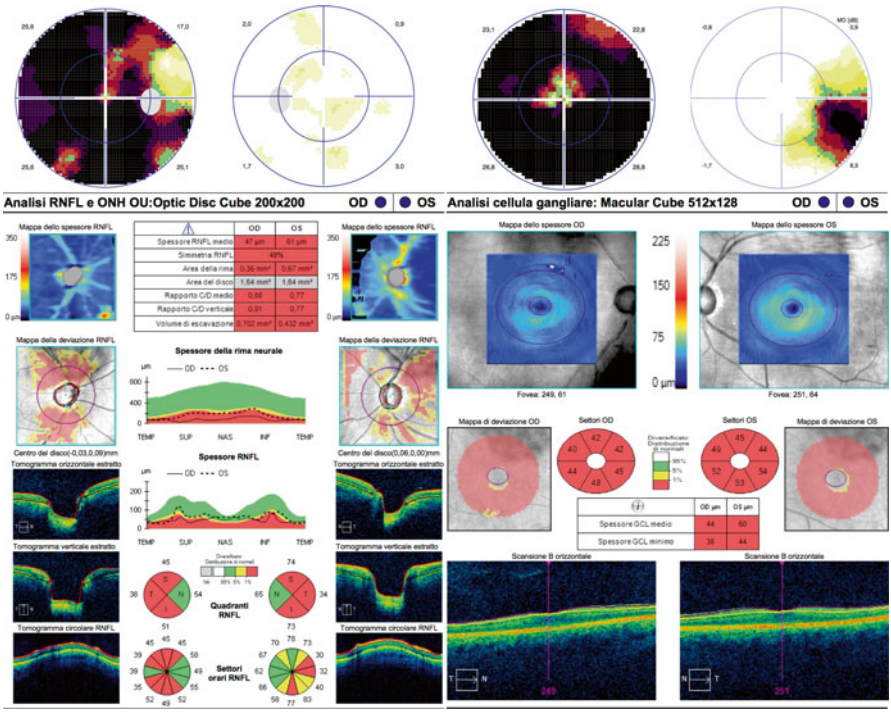

Fig. 9.34 Alterations of ONH, RNFL and GCC parameters in the right eye are at a maximum and congruous with damage detected by white-on-white Octopus perimetry. In the left eye, by contrast, structural damage is much more evident, providing an indication of the evolution of functional damage over time

9.4 Lamina Cribrosa Assessment

In glaucoma, functional damage affects the axons of retinal ganglion cells and this damage is thought to begin in the lamina cribrosa (LC). The pathology of the disease is not yet completely understood and to improve diagnosis and prognosis we need to know the effects of intraocular pressure on the biomechanics of the LC and the surrounding sclera. In recent years, OCT has been used to obtain in vivo images of deep ONH structures, especially the LC. OCT images of the LC are acquired with a deeper focal plane than the optimal plane for RNFL images. This means that traditional ONH images used to analyse RNFL thinning and thickness often do not give optimal visualisation of the LC. A technique known as enhanced depth imaging (EDI) has been developed to improve visualisation of deeper structures, such as the choroid and LC (Fig. 9.35). Available EDI-OCT instruments often use the mean of many photograms to see deeper tissue. To maintain reasonable image-acquisition times, these instruments use radial models and a certain distance between B-scans. In this way, it is possible to see posterior deformation of the LC and its posterior displacement with respect to the sclera. This technique is developing fast and will make it possible to visualise deep ONH components, though the resolution and contrast of OCT images are still less than those, for example, of RNFL images. Moreover, detection of the posterior surface of the LC is still highly variable even with EDI-OCT, as this surface is difficult to identify. Large areas of the LC also remain difficult to visualise. Much work is still necessary, comparing detection of the posterior surface of the LC by OCT with histological images from humans and primates. At the present time, the proliferation of articles on the topic could lead to premature introduction of LC thickness measures into clinical practice.

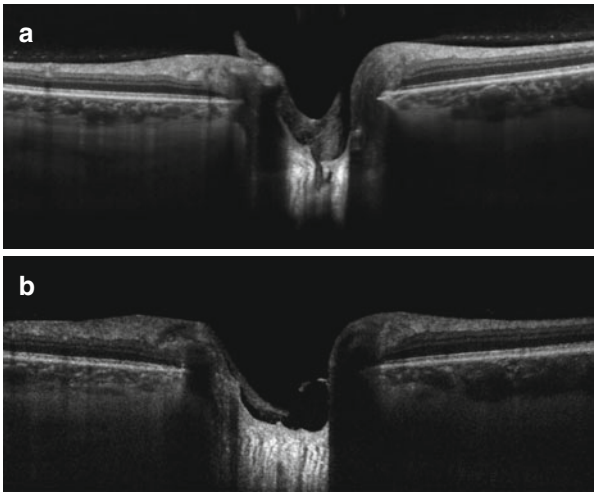

Fig. 9.35 EDI-OCT images use the mean of many photograms to see deeper tissue. In the image a is shown the lamina cribrosa of a normal subject; in the image b is shown a POAG patient with an evident deformation of the lamina cribrosa

Further Reading

1. Rao HL, Zangwill LM, Weinreb RN, Leite MT, Sample PA, Medeiros FA (2011) Structure-function relationship in glaucoma using spectral-domain optical coherence tomography. Arch Ophthalmol 129:864–871
2. Paunescu LA, Schuman JS, Price LL et al (2004) Reproducibility of nerve fiber thickness, macular thickness, and optic nerve head measurements using Stratus OCT. Invest Ophthalmol Vis Sci 45(6):1716–1724
3. Budenz DL, Chang RT, Huang X, Knighton RW, Tielsch JM (2005) Reproducibility of retinal nerve fiber thickness measurements using the Stratus OCT in normal and glaucomatous eyes. Invest Ophthalmol Vis Sci 46(7):2440–2443
4. Tzamalis A, Kynigopoulos M, Schlote T, Haefliger I (2009) Improved reproducibility of retinal nerve fiber layer thickness measurements with the repeat-scan protocol using the Stratus OCT in normal and glaucomatous eyes. Graefes Arch Clin Exp Ophthalmol 247(2):245–252
5. Smith M, Frost A, Graham CM, Shaw S (2007) Effect of pupillary dilatation on glaucoma assessments using optical coherence tomography. Br J Ophthalmol 91(12):1686–1690
6. Budenz DL, Fredette MJ, Feuer WJ, Anderson DR (2008) Reproducibility of peripapillary retinal nerve fiber thickness measurements with Stratus OCT in glaucomatous eyes. Ophthalmology 115(4):661–666
7. Barkana Y, Burgansky-Eliash Z, Gerber Y et al (2009) Interdevice variability of the Stratus optical coherence tomography. Am J Ophthalmol 147(2):260–266
8. Cheung CY, Leung CK, Lin D, Pang CP, Lam DS (2008) Relationship between retinal nerve fiber layer measurement and signal strength in optical coherence tomography. Ophthalmology 115(8):1347–1351
9. Mwanza JC, Chang RT, Budenz DL, Durbin MK, Gendy MG, Shi W, Feuer WJ (2010) Reproducibility of peripapillary retinal nerve fiber layer thickness and optic nerve head parameters measured with cirrus HD-OCT in glaucomatous eyes. Invest Ophthalmol Vis Sci 51(11):5724–5730
10. Vizzeri G, Weinreb RN, Gonzalez-Garcia AO, Bowd C, Medeiros FA, Sample PA, Zangwill LM (2009) Agreement between spectral-domain and time-domain OCT for measuring RNFL thickness. Br J Ophthalmol 93(6):775–781, 50. González-García AO, Vizzeri G, Bowd C, Medeiros FA, Zangwill LM, Weinreb RN (2009) Reproducibility of RTVue retinal nerve fiber layer thickness and optic disc measurements and agreement with Stratus optical coherence tomography measurements. Am J Ophthalmol 147(6):1067–1074
11. Kim JS, Ishikawa H, Sung KR et al (2009) Retinal nerve fiber layer thickness measure- ment reproducibility improved with spectral domain optical coherence tomography. Br J Ophthalmol 93(8):1057–1063, 52. Leung CK, Cheung CY, Weinreb RN et al (2009) Retinal nerve fiber layer imaging with spectral-domain optical coherence tomography: a variability and diagnostic per- formance study. Ophthalmology 116(7):1257–1263
12. Menke MN, Knecht P, Sturm V, Dabov S, Funk J (2008) Reproducibility of nerve fiber layer thickness measurements using 3D fourier-domain OCT. Invest Ophthalmol Vis Sci 49(12):5386–5391, 54. Garas A, Vargha P, Hollo G (2010) Reproducibility of RNFL and macular thickness meas- urements with RTVue-100 optical coherence tomograph. Ophthamology 117(4):738–746
13. Moreno-Montañés J, Olmo N, Alvarez A, García N, Zarranz-Ventura J (2010) Cirrus high-definition optical coherence tomography compared with Stratus optical coher- ence tomography in glaucoma diagnosis. Invest Ophthalmol Vis Sci 51(1):335–343
14. Seibold LK, Mandava N, Kahook MY (2010) Comparison of retinal nerve fiber layer thickness in normal eyes using time-domain and spectral-domain optical coherence tomography. Am J Ophthalmol 150(6):807
15. Sung KR, Kim DY, Park SB, Kook MS (2009) Comparison of retinal nerve fiber layer thickness measured by Cirrus HD and Stratus optical coherence tomography. Ophthalmology 116(7):1264–1270

16. Knight OJ, Chang RT, Feuer WJ, Budenz DL (2009) Comparison of retinal nerve fiber layer measurements using time domain and spectral domain optical coherent to- mography. Ophthalmology 116(7):1271–1277
17. Sehi M, Grewal DS, Sheets CW, Greenfield DS (2009) Diagnostic ability of Fourier- domain vs time-domain optical coherence tomography for glaucoma detection. Am J Ophthalmol 148(4):597–605
18. Mwanza JC, Oakley JD, Budenz DL et al (2011) Ability of Cirrus HD-OCT optic nerve head parameters to discriminate normal from glaucomatous eyes. Ophthalmology 118(2):241–248
19. Jeoung JW, Park KH (2010) Comparison of Cirrus OCT and Stratus OCT on the abil- ity to detect localized retinal nerve fiber layer defects in preperimetric glaucoma. Invest Ophthalmol Vis Sci 51(2):938–945
20. Park S, Sung K, Kang S et al (2009) Comparison of diagnostic glaucoma capabilities of Cirrus HD and stratus optical coherence tomograph. Arch Opththalmol 127(12):1603–1609
21. Sakata LM, Lavanya R, Friedman DS et al (2008) Comparison of gonioscopy and anterior segment ocular coherence tomography in detecting angle closure in different quadrants of the anterior chamber angle. Ophthalmology 115(5):769–774
22. Barkana Y, Dorairaj SK, Gerber Y, Liebmann JM, Ritch R (2007) Agreement between gonioscopy and ultrasound biomicroscopy in detecting iridotrabecular apposition. Arch Ophthalmol 125(10):1331–1335
23. Konstantopoulos A, Hossain P, Anderson DF (2007) Recent advances in ophthalmic anterior segment imaging: a new era for ophthalmic diagnosis?". Br J Ophthalmol 91(4):551–557
24. Radhakrishnan S, Rollins AM, Roth JE et al (2001) Realtime optical coherence tomography of the anterior segment at 1310 nm. Arch Ophthalmol 119(8):1179–1185
25. Radhakrishnan S, Goldsmith J, Huang D et al (2005) Comparison of optical coherence tomography and ultrasound biomicroscopy for detection of narrow anterior chamber angles. Arch Ophthalmol 123(8):1053–1059
26. Leung CKS, Li H, Weinreb RN et al (2008) Anterior chamber angle measurement with anterior segment optical coherence tomography: a comparison between slit lampOCT and visante OCT. Invest Ophthalmol Vis Sci 49(8):3469–3474
27. Sakata LM, Wong TTL, Wong HT et al (2010) Comparison of Visante and slit-lamp anterior segment optical coherence tomography in imaging the anterior chamber angle. Eye 24(4): 578–587
28. Li H, Leung CKS, Cheung CYL et al (2007) Repeatability and reproducibility of anterior chamber angle measurement with anterior segment optical coherence tomography. Br J Ophthalmol 91(11):1490–1497
29. Aptel F, Beccat S, Fortoul V, Denis P (2011) Biometric analysis of pigment dispersion syndrome using anterior segment optical coherence tomography. Ophthalmology 118(8):1563–1570
30. Singh M, Chew PTK, Friedman DS et al (2007) Imaging of trabeculectomy blebs using anterior segment optical coherence tomography. Ophthalmology 114(1):47–53
31. Leung CKS, Yick DWF, Kwong YYY et al (2007) Analysis of bleb morphology after trabeculectomy with Visante anterior segment optical coherence tomography. Br J Ophthalmol 91(3):340–344
32. Ishikawa H, Stein DM, Wollstein G, Beaton S, Fujimoto JG et al (2005) Macular segmentation with optical coherence tomography. Invest Ophthalmol Vis Sci 46:2012–2017
33. Tan O, Li G, Lu AT-H, Varma R, Huang D (2008) Mapping of macular substructures with optical coherence tomography for glaucoma diagnosis. Ophthalmology 115:949–956
34. Tan O, Chopra V, Lu AT-H, Schuman JS, Ishikawa H et al (2009) Detection of macular ganglion cell loss in glaucoma by Fourier-domain optical coherence tomography. Ophthalmology 116:2305–2314.e 2301–2302.
35. Kim NR, Lee ES, Seong GJ, Kim JH, An HG et al (2010) Structure-function relationship and diagnostic value of macular ganglion cell complex measurement using Fourier-domain OCT in glaucoma. Invest Ophthalmol Vis Sci 51:4646–4651
36. Raza AS, Cho J, de Moraes CGV, Wang M, Zhang X et al (2011) Retinal ganglion cell layer thickness and local visual field sensitivity in glaucoma. Arch Ophthalmol 129:1529–1536

37. Shin HY, Park HY, Jung KI, Park CK (2013) Comparative study of macular ganglion cell inner plexiform layer and retinal nerve fiber layer measurement: structure-function analysis. Invest Ophthalmol Vis Sci 54(12):7344–7353
38. Takahashi M, Omodaka K, Maruyama K, Yamaguchi T, Himori N et al (2013) Simulated visual fields produced from macular RNFLT data in patients with glaucoma. Curr Eye Res 38:1133–1141
39. Sato S, Hirooka K, Baba T, Tenkumo K, Nitta E et al (2013) Correlation between the ganglion cell-inner plexiform layer thickness measured with cirrus HD-OCT and macular visual field sensitivity measured with microperimetry. Invest Ophthalmol Vis Sci 54:3046–3051
40. Akagi T, Hangai M, Takayama K, Nonaka A, Ooto S et al (2012) In vivo imaging of lamina cribrosa pores by adaptive optics scanning laser ophthalmoscopy. Invest Ophthalmol Vis Sci 53:4111–4119
41. Inoue R, Hangai M, Kotera Y, Nakanishi H, Mori S et al (2009) Threedimensional high-speed optical coherence tomography imaging of lamina cribrosa in glaucoma. Ophthalmology 116:214–222
42. Ivers KM, Li C, Patel N, Sredar N, Luo X et al (2011) Reproducibility of measuring lamina cribrosa pore geometry in human and nonhuman primates with in vivo adaptive optics imaging. Invest Ophthalmol Vis Sci 52:5473–5480
43. Lee EJ, Kim T-W, Weinreb RN, Suh MH, Kang M et al (2012) Three-dimensional evaluation of the lamina cribrosa using spectral-domain optical coherence tomography in glaucoma. Invest Ophthalmol Vis Sci 53:198–204
44. Kiumehr S, Park SC, Syril D, Teng CC, Tello C et al (2012) In vivo evaluation of focal lamina cribrosa defects in glaucoma. Arch Ophthalmol 130:552–559
45. Nadler Z, Wang B, Wollstein G, Nevins JE, Ishikawa H et al (2013) Automated lamina cribrosa microstructural segmentation in optical coherence tomography scans of healthy and glaucomatous eyes. Biomed Opt Express 4:2596–2608